Upper mantle *P* structure on the ocean side of the Japan–Kurile Arc

Yoshio Fukao* *Department of Earth Sciences, Nagoya University, Chikusa, Nagoya, Japan*

Summary. Slowness measurements are made for the first and later arrivals of *P* waves from about seventy Kurile–Kamchatka earthquakes ($13° < \Delta < 30°$) at the Wakayama Micro-Earthquake Observatory, Japan. The experimental error of $dT/d\Delta$ is not more than 3 per cent and the data points suffice to draw a $dT/d\Delta$ curve fairly uniquely. In the distance range $4° < \Delta < 15°$ a travel-time curve, including a later arrival branch, is constructed for a specific Kurile event using the records along the Pacific coasts of the Japanese–Kurile islands. The results are inverted to obtain a velocity model for the upper 800 km of the mantle beneath the trench side of the Japan–Kurile Arc. The model includes a high-velocity lid extending down to 85 km depth. The low-velocity zone is of relatively high speed (8.1 km/s) and is terminated by a high-velocity gradient zone at depths 165–200 km, just below which the velocity is nearly constant with depth. The velocity increases very sharply near 400 km by about 6 per cent. An abrupt change in the slope of velocity occurs near 520 km. A major transition zone in the depth range 630–670 km consists of about 7 per cent increase in velocity and is sharp, especially near the base. A minor transition zone is tentatively suggested to exist around 740 km. Relative arrival times, crossover distances and qualitative amplitude behaviour calculated for this model are consistent with the observed data. Station residuals for the least-squares determination of $dT/d\Delta$ closely correlate with the local seismicity.

1 Introduction

The most direct evidence about the velocities of compressional waves in the upper mantle comes from travel time, T, or slowness, $dT/d\Delta$, studies of *P* waves at epicentral distances of less than 30°. A number of different upper mantle models have been generated from these studies. The differences can be partly attributed to a regional effect but some of them are undoubtedly due to the difficulties in the interpretation of the observed data. Such difficulties arise from the discrete nature of the data points, through which sometimes a broad

* Present address: Seismological Laboratory, California Institute of Technology, Pasadena, California 91125, USA.
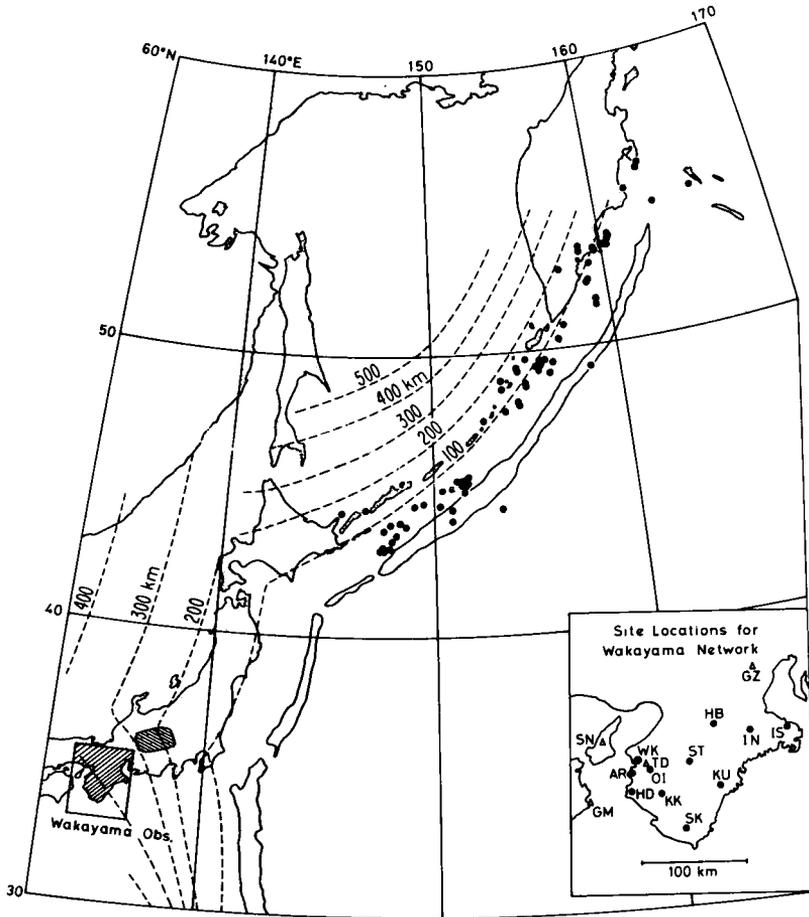
Figure 1. Epicentres for earthquakes listed in Table 1 and contours of the deep seismic zones. Site locations for the Wakayama Micro-Earthquake Observatory are given in the insert. Circles indicate permanent stations. Shaded area shows the horizontal projection of the spots at which rays intersect the Izu—Mariana deep seismic zone.

range of travel-time or slowness curves can be drawn. Each curve will give a different velocity model. To reduce this ambiguity we have made a slowness measurement in an effort to locate as accurately as possible the positions of the later arrival branches and cusps.

Measurements are made for P waves, at the Wakayama Micro-Earthquake Observatory in the Kii peninsula, Japan, exclusively from earthquakes in the Kurile—Kamchatka region. The travel paths are largely confined to the oceanic side (trench-side) of the deep seismic zone of the Japan—Kurile arc as may be inferred from Fig. 1. The epicentral distances Δ range from 13 to 30°. This slowness study may be compared in many aspects to the travel time study by Kishimoto (1956) who used about twenty JMA (Japan Meteorological Agency) stations at the Pacific side of the Japanese islands for several Kurile—Kamchatka earthquakes.

2 Data

Kanamori (1967) was the first who used the Wakayama Network as a seismic array to derive a velocity model for the mantle beneath Japan. Details of the network are given in Kanamori's paper. In short, it is an eleven-element short-period vertical seismometer net

Table 1. Earthquake list and slowness data.

Event No.	Day	Month	Year	h	m	s	Δ deg	Azimuth deg	h km	Δ_c deg	p s/deg	S.D. s/deg	Type of Arrival
1*	11	01	65	22	47	06.3	19.71	37	102	20.81	11.31	–	F
2*	11	03	65	08	31	01.3	16.03	41	49	16.62	12.76	–	F
3*	28	03	65	13	22	57.6	27.95	33	33	28.11	8.74	–	F
4*	05	04	65	13	52	13.4	15.86	44	81	17.14	12.87	–	F
5	24	10	65	18	15	10.3	21.45	38	73	22.07	10.50	0.24	F
6	25	10	65	22	34	22.4	12.28	34	159	15.39	12.72	0.32	F
7	18	01	67	04	20	55.0	20.30	38	58	20.83	11.19	0.22	F
8	02	03	67	23	03	44.2	26.13	34	57	26.46	8.81	0.22	F
9	19	03	67	04	01	38.5	16.21	41	38	16.51	11.50	0.20	L
10	20	03	67	13	31	33.8	16.35	42	46	16.77	11.64	0.16	L
11	20	03	67	13	40	51.2	16.42	42	35	16.71	11.95	0.16	L
12	20	03	67	13	52	03.7	16.39	42	23	16.55	11.53	0.13	L
13	25	03	67	22	47	58.4	16.19	43	47	16.61	11.53	0.16	L
14	01	04	67	05	54	19.8	16.60	42	49	17.05	11.57	0.16	L
15	01	04	67	12	23	34.6	16.51	42	36	16.80	11.77	0.11	L
16	04	06	67	05	26	47	24.10	38	24	24.23	9.59	0.21	F
										24.22	9.12	0.08	L
17	02	08	67	00	44	39.4	13.18	36	131	15.71	12.87	0.34	F
18	10	08	67	11	21	22.7	15.61	41	44	16.00	11.56	0.14	L
19	30	08	67	13	33	24.2	16.32	42	17	16.44	11.62	0.20	L
20	07	10	67	08	27	59.5	21.18	39	22	21.33	11.00	0.23	F
21	01	11	67	16	09	17.0	19.67	39	50	20.09	11.11	0.15	LF
22	01	11	67	16	30	58.4	19.66	39	52	20.10	11.09	0.15	LF
23	01	12	67	13	57	03.4	20.45	36	144	21.95	10.86	0.37	F
										21.58	9.50	0.09	L
										22.58	12.15	0.12	L
24	13	12	67	10	38	25.3	18.39	38	142	19.99	11.20	0.21	LF
										19.44	9.18	0.17	L
25	13	12	67	10	58	22.2	20.42	37	144	21.90	10.80	0.27	F
										21.53	9.40	0.16	L
										22.64	12.26	0.13	L
26	29	02	68	15	46	19.0	24.14	33	160	25.31	9.04	0.12	F
27	20	05	68	10	34	18.8	20.27	39	55	20.78	11.32	0.14	F
										20.63	9.33	0.18	L
28	20	05	68	21	09	45.4	15.18	42	44	15.57	11.60	0.12	L
29	03	06	68	14	16	18.4	14.80	37	152	17.89	12.83	0.14	F
										16.78	11.69	0.18	L
30	24	10	68	22	35	54.0	21.29	38	62	21.86	11.13	0.20	F
										21.69	9.17	0.10	L
										21.70	9.42	0.13	L
31	15	12	68	14	01	46.5	21.18	38	79	21.86	10.45	0.23	F
32	19	12	68	15	15	58.7	25.79	35	51	26.09	8.97	0.12	F
33	20	01	69	14	20	10.6	29.39	36	17	29.46	8.66	0.15	F
34	22	01	69	00	42	31.4	28.59	33	46	28.84	8.74	0.20	F
35	31	01	69	04	10	23	25.10	33	112	25.86	8.92	0.19	F
36	03	02	69	08	57	08.9	20.98	38	54	21.41	10.59	0.15	F
										21.33	9.38	0.10	L
37	03	03	69	14	49	31.6	24.21	37	38	24.42	9.20	0.12	F
38	18	03	69	16	16	39.4	15.21	45	45	15.60	11.47	0.13	L
39	08	06	69	14	49	33.0	25.47	34	74	25.94	8.96	0.12	F
40	13	06	69	08	48	28.3	20.99	38	52	21.41	10.74	0.23	F
41	22	06	69	02	33	51.9	22.44	41	24	22.59	10.42	0.26	F
42	16	07	69	08	16	50.4	24.44	36	44	24.69	9.12	0.15	LF
										24.72	9.79	0.13	F

Table 1 – *continued*

Event No.	Date Day	Month	Year	Origin time h	m	s	Δ deg	Azimuth deg	h km	Δ_c deg	p s/deg	S.D. s/deg	Type of Arrival
43	07	08	69	06	46	06.7	24.46	36	52	24.78	9.09	0.10	F
										24.82	9.91	0.11	L
										24.85	10.32	0.11	L
44	12	08	69	05	03	30.5	13.16	42	70	13.84	11.31	0.15	L
45	12	08	69	11	21	23.3	13.82	42	39	14.14	11.44	0.16	L
46	13	08	69	08	31	33.1	13.40	40	41	13.84	12.72	0.32	F
47	13	08	69	22	57	08.3	13.72	41	36	14.07	12.71	0.30	F
48	14	08	69	14	19	03.6	12.66	42	46	13.28	13.24	0.18	F
49	15	08	69	04	32	02.1	12.87	42	40	13.33	13.08	0.29	F
50	16	08	69	15	15	30.9	12.66	42	49	13.32	13.09	0.18	F
51	16	08	69	17	13	42.6	12.68	42	48	13.36	13.28	0.31	F
52	19	08	69	08	49	54.3	13.34	42	39	13.75	12.88	0.25	F
										13.64	11.22	0.10	L
53	20	08	69	07	50	09.8	19.10	39	111	20.27	11.14	0.13	F
54	23	01	70	22	22	37.9	20.91	37	122	22.06	10.54	0.16	F
55	06	02	70	00	11	49.5	28.06	35	43	28.31	8.95	0.19	F
56	10	03	70	04	58	26.7	14.49	40	44	15.02	12.88	0.28	F
57	10	06	70	16	17	48.1	14.79	41	53	15.28	11.44	0.12	L
58	28	06	70	11	01	56.2	25.85	35	44	26.10	8.83	0.20	F
59	28	09	70	17	22	13.6	25.05	33	133	25.98	8.91	0.11	F
60	08	10	70	04	53	19	26.14	34	30	26.29	8.77	0.18	F
61	08	10	70	23	36	11.6	13.08	40	28	13.35	13.27	0.26	F
62	01	08	71	02	06	10.0	22.25	37	43	22.56	10.44	0.19	F
63	24	11	71	19	35	28.5	24.97	35	99	25.63	8.88	0.13	F
64	02	12	71	17	18	24.0	17.04	47	38	17.42	12.68	0.15	F
										17.33	11.19	0.20	L
65	15	12	71	08	29	56.6	28.78	32	39	28.98	8.68	0.15	F
66	22	03	72	10	27	42.1	19.79	36	135	21.23	11.00	0.14	F
67†	27	11	73	13	52	29.6	26.17	34	60	26.52	8.79	0.08	F
68†	26	02	74	06	23	45.3	25.48	34	49	25.77	9.06	0.18	F
										25.81	9.85	0.11	L
69†	27	05	74	04	41	23.6	22.74	37	47	23.12	10.86	0.23	F
										23.05	9.75	0.13	L

F: First arrivals, L: Later arrivals, LF: Later to first arrivals.
* Kanamori's (1967) data for Kurile–Kamchatka earthquakes with the focal coordinates given by USCGS.
† NOAA locations. For other events ISC locations are used.

whose linear extent is 130–140 km for the earthquakes used here. The site locations are plotted on the map in the insert of Fig. 1.

Sixty-five events are selected from a list of Kurile–Kamchatka earthquakes. Most of them occurred in the interval of 1967 January to 1970 December. Among the earthquakes studied by Kanamori (1967) four are the Kurile–Kamchatka events. They are included in this study. The epicenter locations are shown in Fig. 1. The hypocentre data in Table 1 are mostly from ISC locations. For a few latest earthquakes the ISC data are not available. The NOAA data are used in these cases since the recent ISC and NOAA locations give approximately the same epicenter. The errors in hypocenter determinations have anyway little effect in the $dT/d\Delta$ determination. The distance Δ given in Table 1 is the simple average of those for the nearest and the furthest stations of the net.

3 Analysis

For each event the original seismograms from all the stations are copied and pasted up to see the coherence of signal waveform. The initial onsets are read on these copies to 0.1 s in most

69 AUG 12, 05h03m30.5s, H = 70 km

Δ = 13.16°,   φ = 42°

IS

IN

HB

├─10 sec─┤

1°

KU
ST

OI
WK

KK
AR

SK

HD

JB P due   P = 11.31 sec/deg
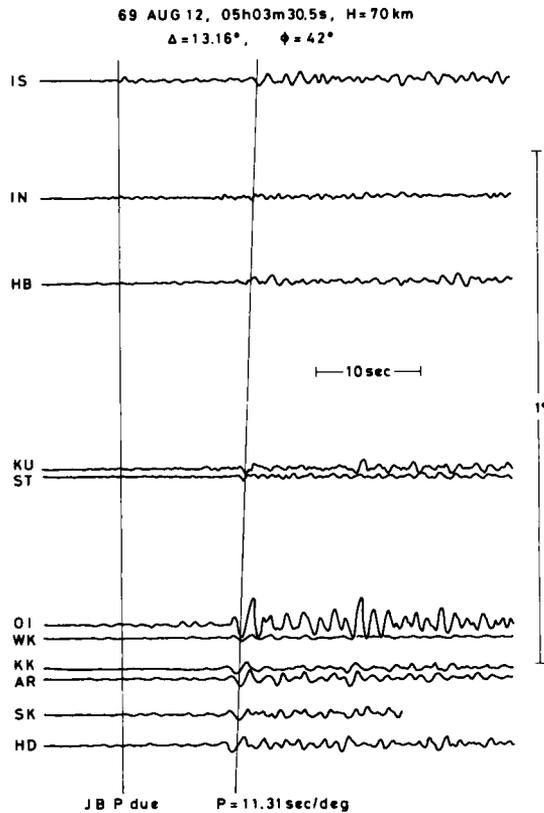
Figure 2. Seismograms for Event 44. *P* phase arrives a few seconds before JB time but the commencement is not clear.

cases and to 0.01 s for very good signals. For later phases relative arrival times are measured to 0.1 to 0.01 s using, in general, the first prominent peak or the first definite zero crossing of the waveform (Johnson 1967). The slowness $p = dT/d\Delta$ is then determined by a least-squares procedure and, using its value, the distance Δ and the travel time T are corrected to surface focus for each of the first and later arrivals. The above correction is made with the Jeffreys velocity structure. The arrivals which can be identified as pP on the basis of slowness and travel time are discarded.

No correction is made for dipping interfaces beneath the net. The effect of the Moho, which dips toward north, is to reduce the slowness by a factor of 1−2 per cent for seismic waves considered here (Kanamori 1967; Niazi 1966). The effect of a deeper dipping interface may be more serious. The Wakayama Observatory is situated above the deep seismic zone associated with the Izu−Mariana arc (see Fig. 1). The zone dips toward south-west at an angle of about 40°. The dip direction is approximately the same as the propagation azimuth of the ray. Although the seismic zone is characterized by an anomalously high velocity (e.g. Utsu 1971), it would not significantly affect the slowness measurement if there were no velocity contrast between the two parts of the mantle separated by it. Utsu (1971) and Hamada (1973), however, pointed out that the oceanic side of the mantle is a few per cent faster than the other side of the mantle. If the velocity contrast is 3 per cent according to Hamada (1973), the slowness will be increased by a factor of 2−3 per cent. The net effect for the two dipping interfaces is therefore an increase of the slowness by a factor of 1−2 per cent which is less than the observation error. The remaining major portion of the ray path is

67 APR 01, 12h23m34.6s, H = 36km
Δ = 16.51°,   φ = 42°

71 DEC 02, 17h18m24.0s, H = 38 km
Δ = 17.04°,   φ = 47°
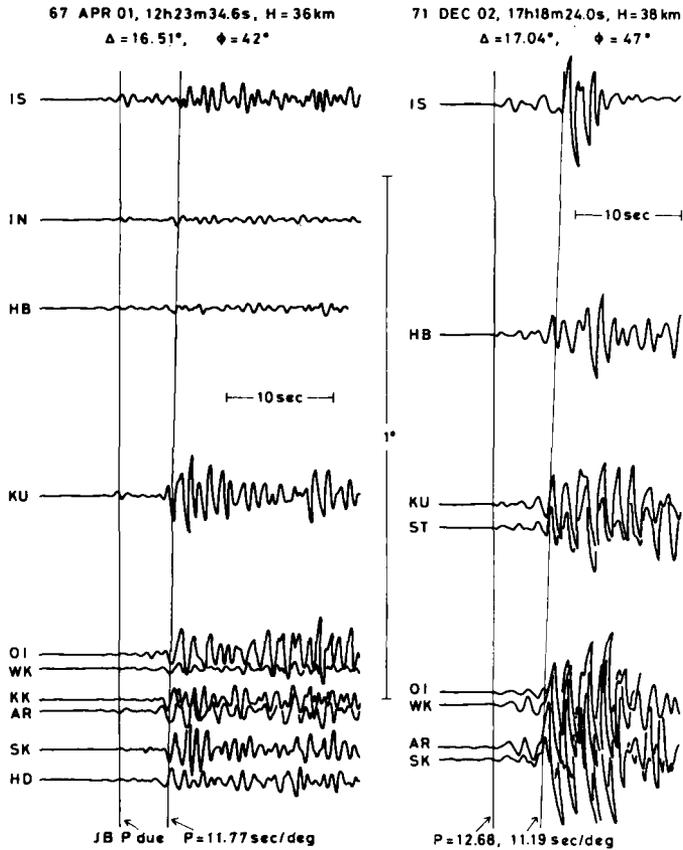
Figure 3.   (Left) seismograms for Event 15. *P* phase arrives a few seconds before JB time but the commencement is not clear. (Right) seismograms for Event 64. An abrupt reduction of amplitude at IS is due to automatic gain controlling. Seismograms at KK and HD are not shown to avoid the complexity of illustration. Seismograms at AR and SK are subject to noise disturbance.

67 DEC 13, 10h38m25.3s, H = 142km
Δ = 18.39°,   φ = 38°

68 MAY 20, 10h34m18.8s, H = 55km
Δ = 20.27°,   φ = 39°
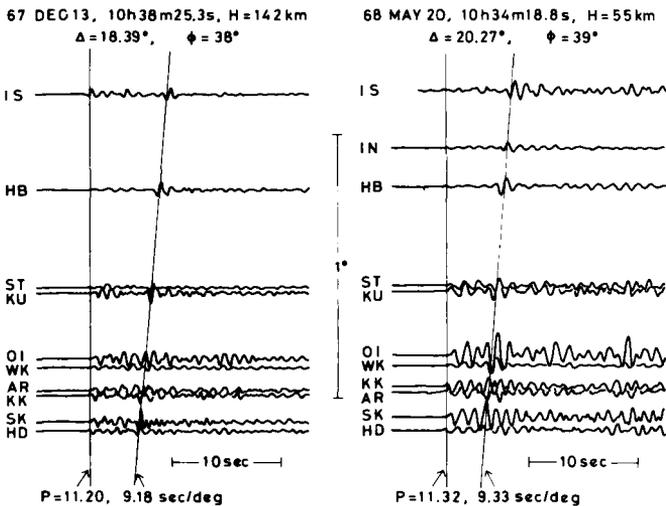
Figure 4.   (Left) seismograms for Even 24. (Right) seismograms for Event 27. Seismogram at IS is subject to noise disturbance. The first motion at HB is overlapped by the time mark.

67 DEC 13, 10h58m22.2s, H=144 km
Δ = 20.42°,   φ = 37°

68 OCT 24, 22h35m54.0s, H=62km
Δ = 21.29°,   φ = 38°

P=10.80, 9.40,12.26 sec/deg

P=11.13, 9.17, 9.42 sec/deg
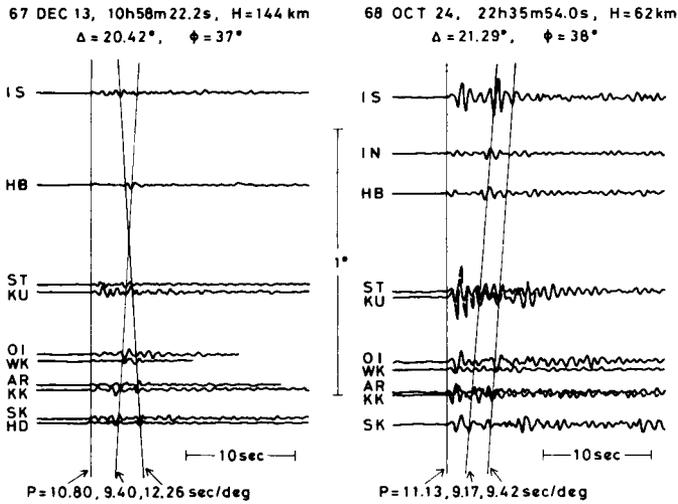
Figure 5. (Left) seismograms for Event 26. (Right) seismograms for Event 30.

69 AUG 07, 6h46m06.7s, H=52km
Δ = 24.46°,   φ = 36°

69 JUN 08, 14h49m33.0s, H=74km
Δ = 25.47°,   φ = 35°

P=9.09, 10.32, 9.91 sec/deg

P=8.96 sec/deg
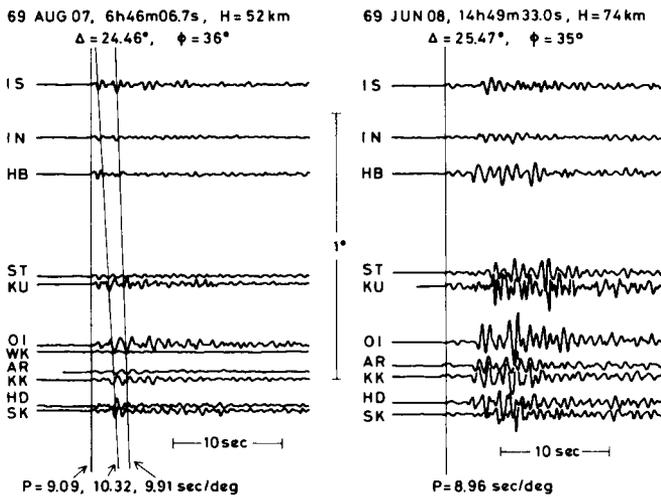
Figure 6. (Left) seismograms for Event 43. (Right) seismograms for Event 39. The first motion at AR and KK is overlapped by the time mark.

almost parallel to the tectonic trend of the island arcs so that the propagation azimuth would be little affected by the lateral heterogeneity of the arcs. The above discussion may not be appreciable to the rays grazing the uppermost part of the mantle because they might be affected in a complex way by one or more seismic zones. In fact we found some scatter in the $dT/d\Delta$ values at shortest epicentral distances ($\Delta \sim 13°$). The scatter may be attributed to the complex path effect although other explanations are possible. We will not rely too much on the $dT/d\Delta$ values obtained at these distances.

Several examples of the array seismograms are shown in Figs 2–7. In these figures the amplitudes are not normalized with respect to the instrumental magnification which varies from one station to another (Kanamori 1967). A straight line shows the least-squares fit to the relative arrival times of one arrival and gives the slowness of that arrival. The slowness data so obtained are summarized in Table 1 and are plotted in Fig. 8. As can be seen, the
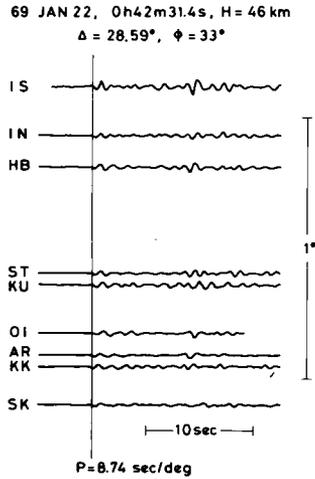
Figure 7.   Seismograms for Event 34.
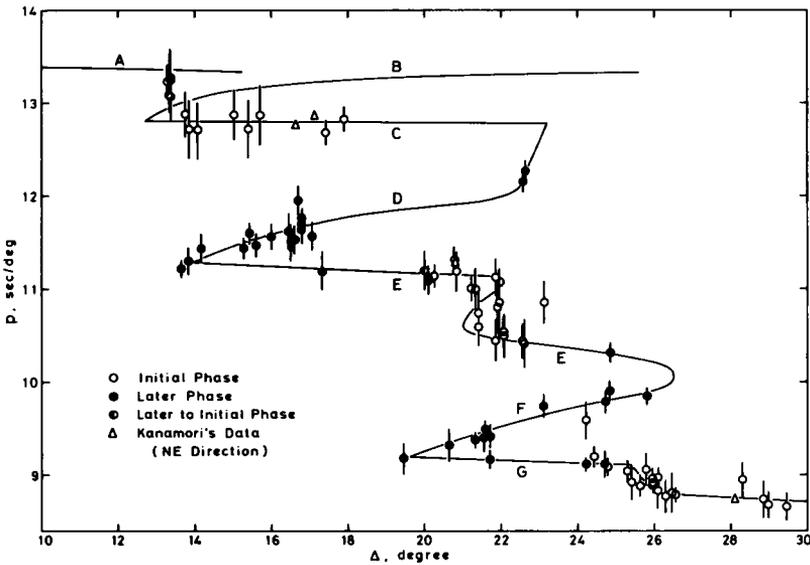
Figure 8.   Measured values of $p=dT/d\Delta$.

standard deviation of the determination is not more than 3 per cent for each arrival. This is consistent with the scatter of the data which are fitted with a continuous curve in Fig. 8. The curve is constructed with the constraints that p must be a monotonically decreasing function and that the amplitudes should be large if $p-\Delta$ curve is steep and should be small if it is flat. Various arrival branches emerge from Fig. 8 and the nomenclature C to G is used to specify each of them. In what follows we explain these branches; Δ always refers to the epicentral distances corrected to surface focus. Note that the uncorrected distances were given in Figs 2–7.

$\Delta = 13-20°$ In the distance range 14–18° the first arrival emerges on the C branch which corresponds to the Pd branch of Kishimoto (1956). This arrival is often too weak to be picked. In figs 2 and 3 (left) the P phase arrives a few seconds before the Jeffreys–Bullen (JB) time at each station but its commencement is by no means clear. Fig. 3 (right) shows a

rather exceptional case where the *C* first arrival can be recognized because of the magnitude of the earthquake. We have collected the records for this event from other stations at smaller distances. The results of the analysis will be given in a later section. The amplitude of the *C* arrival which is already small near 14° becomes smaller and smaller as Δ increases. Such a trend has been first remarked by Kishimoto (1956) who described it as 'abnormally strong diminuation' of *Pd* waves. The slowness of this branch is almost constant, about 12.8 s/deg (Fig. 8). This almost constant slowness well explains the weakness of the *C* arrival and is one of the most important features of Fig. 8.

The weak *C* arrival is usually followed by a much stronger arrival (Figs 2 and 3). Its emergence has been found by Kishimoto (1956) at the uncorrected distance of 13° and then by Kanamori (1967) at 16°. The discrepancy between the two can be attributed to the complicated amplitude behaviour of this arrival. For example, in Fig. 2 the later arrival shows very large amplitude at stations beyond OI (Δ = 14.25°) while in Fig. 3 (left) it does not show very large amplitude up to HB (Δ = 16.85°). Admitting this kind of complexity, we have confirmed the emergence distance to be about 13.5°. The plot of the measured values of *p* versus Δ (Fig. 8) suggests that the observed later arrivals belong, in most cases, to the retrograde branch *D*. No clear records are found that show the separation of the prograde (*E*) branch from the retrograde (*D*) branch.

In the distance range considered here the later arrival data are more abundant than the first-arrival data. This is again a manifestation of the weakness of the *C* arrival. No data are available at distances around 19° where an extensive seismic gap for a great earthquake has been reported (Kelleher, Sykes & Oliver 1973).

20–24°. The *C* first arrival intersects the *E* later arrival at distance near 20° beyond which the *E* branch becomes the first arrival branch. A similar intersection has been reported by Kishimoto (1956) at the uncorrected distance of 18° and by Kanamori (1967) at 19.5°. Fig. 4 (left) shows an example. The *E* arrival is preceded by the *C* arrival at station IS (Δ = 19.36°) but emerges as a clear first arrival at stations beyond KU (Δ = 20.11°). The *C* arrival which was overtaken by the *E* arrival cannot be usually identified because of its weakness. It is also difficult to recognize the extension of *D* beyond 20°. Although the relatively large later arrivals near Δ = 22.5° are identified as being of the *D* branch on the basis of the slowness (Fig. 5, left), more data would be required to confirm this observation. We have tentatively drawn the *dT/d*Δ curve in such a way that the forward extension of the *C* and *D* branches can produce large amplitudes only near 22.5°.

The slowness of the *E* branch rather abruptly changes around 21.5° from about 11.1 to 10.5 s/deg. Correspondingly the amplitudes sometimes become very strong near here. For example, in Fig. 4 (right) the first arrival is relatively weak up to station HB (Δ = 20.51°) but gains strength at larger distances. The *E* phase here sometimes shows an additional complexity, suggesting multiple arrivals separated by about 1 s. In order to explain such a complexity we have drawn the *dT/d*Δ curve to form a very small triplication near 21.5°. This explanation is tentative, however, because other explanations are equally possible. What is essential here is an abrupt decrease in slowness whose detail is beyond the resolving power of the present analysis. The same trend has been formerly observed by Kanamori (1967), although his data are not exclusively from the Kurile–Kamchatka region. The trend is also suggested from Kishimoto's (1956) travel-time data. Fig. 9 plots his data for a branch corresponding to the *E* branch in our notation. It can be seen that the apparent slowness of this branch differs significantly for two slightly different distance ranges.

A new later phase of large amplitude emerges at Δ = 19.5° and it can be traced up to 26° along the retrograde branch *F* (Figs 4 and 5; Fig. 6, left). The observed slownesses are less scattered and the amplitude variation is more systematic as compared to those for the
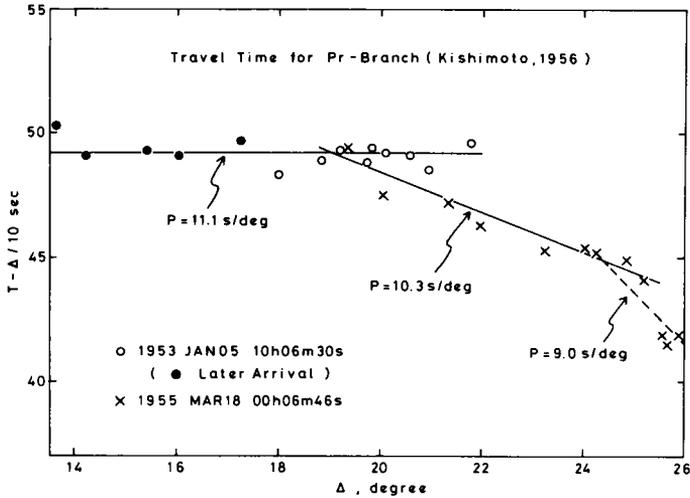
Figure 9. Reduced travel times for two Kamchatka earthquakes (after Kishimoto 1956). Three lines with different slownesses are drawn for reference. Only *Pr* arrivals (Kishimoto 1956) are plotted.

D later arrivals. For some earthquakes it is also possible to recognize the prograde branch *G*. Fig. 5 (right) shows the beginning of the separation of *G* from *F* although here it is in general difficult to determine the accurate slowness separately. It should be noted that Kishimoto (1956) found for *S* waves an emergence of a large later phase at the uncorrected distance of 19° and its intersection with the forerunning *S* phase at about 24°. His observation concerning the *S* waves is remarkably consistent with our result for *P* waves.

24–30°. The *G* arrival intersects the *E* phase at 24–24.5° beyond which the *G* phase becomes the first arrival. Fig. 6 (left) shows the seismograms around 24.8°, where the *G* first arrival is followed by the *E* and then the *F* arrivals. There is no observable indication that these *E* and *F* branches extend much beyond 26°. They can exist up to slightly more than 26°, where the later arrival portion of a seismogram is usually so complicated that it is difficult to measure $dT/d\Delta$ (Fig. 6, right). A rapid decrease in *G* slowness from 9.1 to 8.8 s/deg is found near 26° although the amplitude increase which might be expected from the ray theory is not clearly observed. The seismograms at distances 28–30° show simple *G* arrivals (Fig. 7). Our $dT/d\Delta$ curve coincides with Kanamori's (1967) curve at $\Delta = 30.05°$ where $p = 8.70$ s/deg.

4 Travel-time curve at shorter distances

We now establish the reverse end of the *C* branch and estimate the penetration depth of the ray corresponding to that end. Such estimation is necessary for an inversion of the $dT/d\Delta$ curve obtained in the last section. The use of the Wakayama net is not adequate because of the possible complex path effect. We therefore use a different approach, a travel-time method similar to the one used by Kishimoto (1956).

4.1 DATA

The Kurile earthquake of 1971 December 2, ($mb = 6.2$, $Ms = 6.3$) is particularly suitable for our purpose because it showed clearly the *C* first arrivals at the Wakayama network (Fig. 3, right). The epicentre has been located oceanward of the axis of the Kurile trench (Fig. 10).
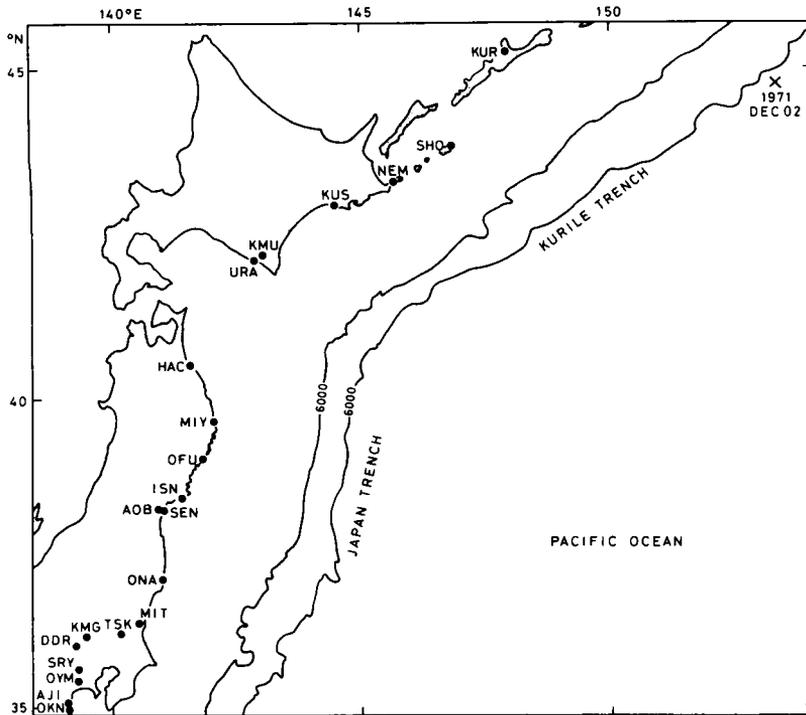
Figure 10. Epicentre of the earthquake of 1971 December 2 (Event 64) and locations of the stations.

The reported origin time is 17 h 18 m 32.8 s, 21.8 s and 24.0 s according to JMA, NOAA, and ISC respectively. Such a large discrepancy is the result of the combining effects of the unfavourable distribution of nearby stations and the lateral heterogeneity associated with the downgoing slab of lithosphere. Although we adopted the ISC determination (Event 64 in Table 1) which was proven to be better than the other two determinations at least for deep and intermediate-depth earthquakes in Japan and Kurile (Utsu 1975), the uncertainty may be still considerable especially in the origin time and the focal depth. We collected the copies of the seismograms from several micro-earthquake observatories and several JMA observatories equipped with electromagnetic seismographs. They are all situated at the Pacific coasts ($\Delta < 13°$) or near the coasts ($\Delta > 13°$) as shown in Fig. 10. The traverse sections are almost uniquely characterized by the deep-sea trench and its landward sea bottom. Epicentral distances are not corrected to surface focus in this section.

4.2 ANALYSIS

The P-wave arrivals are usually marked by a sharp downward motion. Their onset times are read and listed in Table 2. Also added are the reported arrival times of two USSR stations closest to the Pacific Ocean (Fig. 10). The reduced travel times are plotted in Fig. 11 where the data up to 14° are fitted by a straight line giving an apparent velocity of $C = 8.30$ km/s. A relatively large positive deviation at URA and a negative deviation at TSK are perhaps due to the anomalous structure beneath these two stations (Utsu 1975). After a correction of ± 1.0 s at URA and TSK (Utsu 1975, Fig. 6) as shown by the arrows in Fig. 11, the standard deviation of the fitness is 0.19 s while it is 0.40 s without correction. This branch is designated A.

Table 2. The Kurile earthquake of 1971 December 2.

Origin time: 17 h 18 m 24.0 s

Station	Δ deg	Arrival time A m	A s	P′ m	P′ s
KUR	3.91	19	24.1		
SHO	4.77	19	35.1		
NEM	5.77	19	49.0		
KUS	6.70	20	01.4		
KMU	7.95	20	18.0		
URA	8.11	20	21.2		
HAC	9.67	20	40.9		
MIY	9.86	20	43.5		
OFU	10.36	20	50.4		
ISN	11.01	20	59.4		
SEN	11.36	21	03.9		
AOB	11.40	21	04.3		
ONA	12.22	21	– ●		
MIT	12.86	21	23.4	21	27.5
TSK	13.19	21	27.2		
KMG	13.66			21	37.4
DDR	13.87	21	40.2		
SRY	14.09	21	43.0		
OYM	14.25	21	– †	21	45.1
AJI	14.60			21	49.7
OKN	14.69			21	50.9

● The first motion is masked by the background noise.

† Very small amplitude.

The *A* branch does not extend much beyond 14°. The *A* arrival does exist at OYM (Δ = 14.25°) but it is too weak for its onset to be picked (Fig. 12). Instead, a later arrival designated by *p′* is clearly seen. At OKN (Δ=14.69°) the *A* arrival is totally missing and the *P′* is apparently the first arrival. The existence of the *P′* phase can be traced back to MIT (Δ=12.86°) where the *P′* phase emerges 4 s after the *A* arrival. The *A* arrival is weak in the whole distance range where the *P′* phase follows. For example, at KMG (Δ=13.66°) the *A* arrival cannot be observed because of low magnification of JMA seismographs and the *P′* phase is apparently identified as the first arrival. For the same reason the plots of the reported JMA arrivals largely fall on the expected *P′* times rather than on the *A* times at these distances. Fig. 12 shows several seismograms cited in the above discussion. The seismograms at the Wakayama net (Δ∼17°) are shown in Fig. 3 (right), where the first arrivals belong to the *C* branch. If these first arrivals are reduced to smaller distances with the *C* slowness (≃12.8 s/deg), they come to agree with the *P′* arrivals (see Fig. 15). The *C* branch is therefore interpreted as the prograde branch for the *P′* phase.

It has long been recognized that near 13° there is a discontinuous change in travel-time curve for *P* waves from Kurile sources to Japanese stations (Kishimoto 1951; Hirono 1959). Over similar paths, Mizoue & Tsujiura (1974) found a later phase 3–4 s after the first arrival in the distance range 12.5–13°. They also noticed that, although the first arrival branch is quite likely to extend up to some 15°, it is practically impossible to trace its forward extension beyond 13° in most cases because of the small amplitude. All these findings are consistent with the results of the present analysis, which are summarized as follows. (1) The first arrival data up to Δ ∼ 14° can be fitted by a straight line of *C*=8.30±0.01 km/s. (2) This first
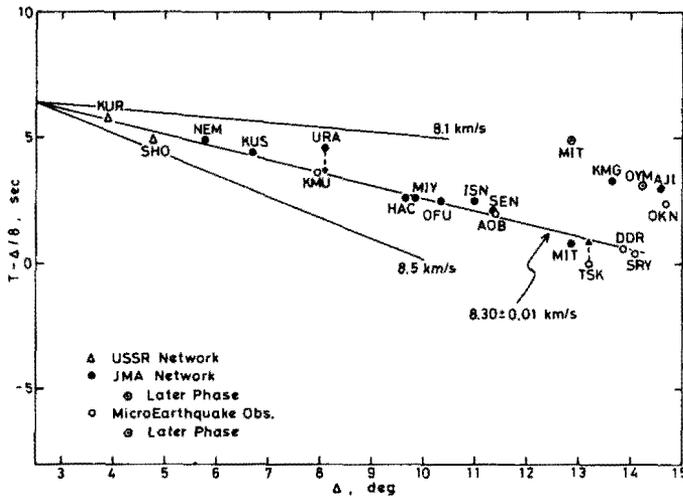
**Figure 11.** Reduced travel times for the earthquake of 1971 December 2. Arrow shows the station correction.
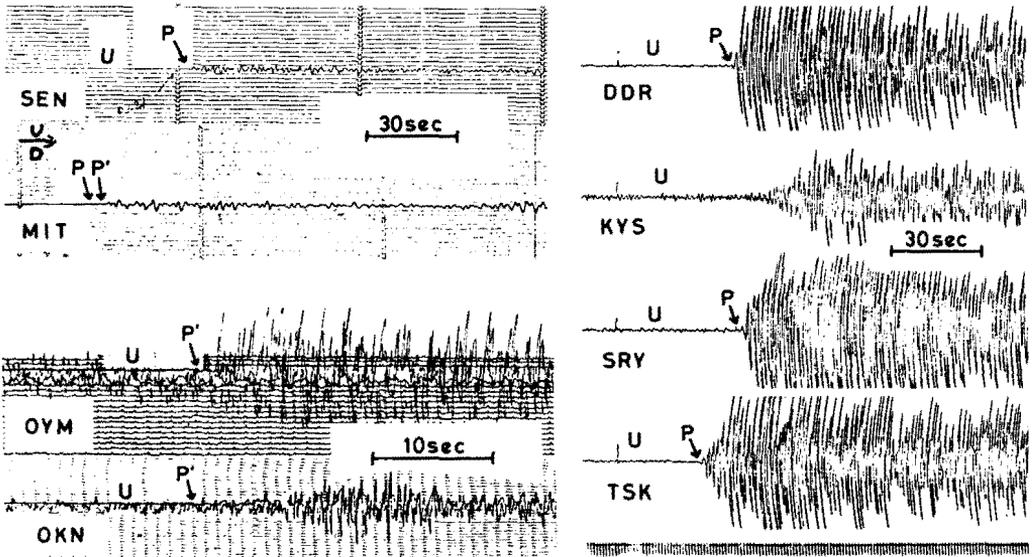
Figure 12. Seismograms in a distance range 11–15°. Stations SEN and MIT belong to JMA and others belong to the Dodaira Micro-Earthquake Observatory. Seismograms at DDR, KYS (not used), SRY and TSK are shown in a strip chart, although the arrival times were read from the original high-speed records.

arrival branch (*A* branch) vanishes near 14.5°. (3) The *C* branch (slowness ≃ 12.8 s/deg) extends backward to a distance of 12.5–13° where the time difference between the *A* and *C* arrivals is about 4 s.

4.3 VELOCITY MODEL

Mizoue & Tsujiura's finding and the observation (3) fix the reverse end of the *C* branch. The corresponding penetration depth can be estimated by constructing a velocity model which satisfies all the above observations. It is obvious from (2) and (3) that any such a model

Table 3. Velocity model ARC–TR.

Depth km	Velocity km/s	Depth km	Velocity km/s
0	5.57	420	9.297
15	5.57	440	9.328
15	6.50	460	9.384
33	6.50	480	9.477
33	8.23	500	9.598
85	8.23	520	9.722
95	8.10	540	9.795
165	8.10	560	9.851
200	8.41	580	9.903
205	8.411	600	9.962
225	8.401	620	10.038
240	8.404	640	10.142
260	8.420	660	10.360
280	8.447	670	10.540
300	8.484	680	10.798
320	8.528	700	10.867
340	8.582	720	10.927
360	8.645	740	11.023
385	8.750	760	11.129
400	9.252	780	11.184
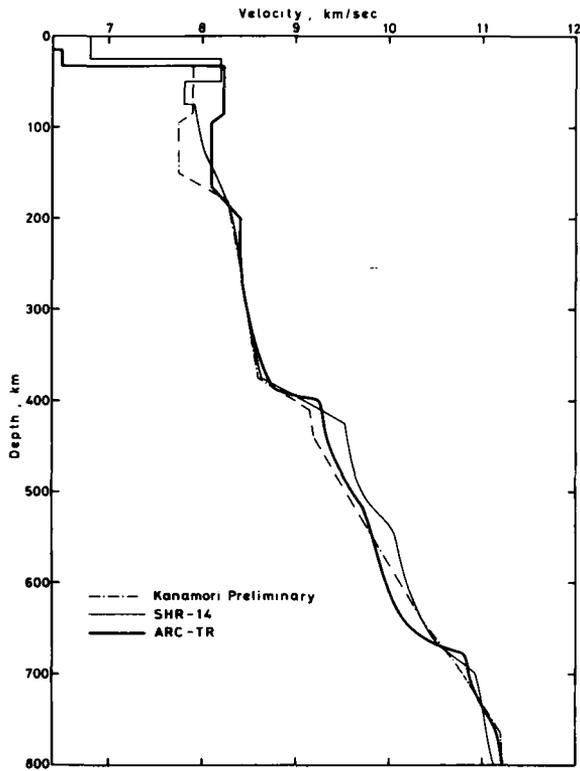
Figure 13. Upper mantle velocity models Preliminary (Kanamori 1967) and SHR14 (Helmberger & Engen 1974) compared with ARC–TR.

should possess a low-velocity layer. Since the fine structure of the low-velocity layer is indeterministic, we assume a simple configuration as shown in Fig. 13. The crustal structure is assumed as in Table 3. With these assumptions the velocity—depth profile can be fairly narrowly constrained and in fact the profile shown in Fig. 13 and Table 3 is the only successful model among many trials.

The model includes a high-velocity lid ($Vp = 8.23$ km/s) extending down to 85 km depth with a low-velocity layer ($Vp = 8.1$ km/s) below it. The base of the low-velocity layer consists of a rapid increase in velocity which starts at 165 km ($Vp = 8.1$ km/s) and terminates at 200 km ($Vp = 8.41$ km/s). This velocity gradient is required from the observation for the reverse end of the C branch and fairly well constrained. Below 200 km a very small negative velocity gradient follows. The theoretical travel times of this model are shown in Fig. 14 where the origin time is shifted by 3.5 s so that they agree with the observed data. The JB times are used as a reference. The agreement is very good except for the above base line shift. It is interesting to note that the ISC origin time is 3.3 s earlier than the actual shot time for the CANNIKIN explosion of 1971 November 6 at the Amchitka island where the tectonic setting is similar to that for the Kurile event. We therefore believe that the requirement of the time shift of 3.5 s is not a manifestation of inadequacy of the model but indicates the actual origin time to be later and/or the actual focal depth to be shallow than those determined by the ISC. The slowness curve calculated for this model defines the whole A and B branches (Fig. 8). The B branch is the later arrival branch due to strong upward refraction at the base of the low-velocity layer. The turning point from B to C corresponds to the ray which bottoms at the depth of 200 km. At some distances around this point the observed slownesses show intermediate values of A and C. This may be explained by either interference between the two close arrivals of the A and P' phases or the complex path effect.

5 Inversion of $dT/d\Delta$ curve

In the last section we have located the reverse end of the C branch. Starting from this point the $dT/d\Delta$ curve is successively integrated by the Herglotz—Wiechert method to obtain a velocity—depth profile below 200 km. This is done after striping the upper 200 km. The result of the inversion is shown in Fig. 13 and Table 3. Note that the uncertainty in the
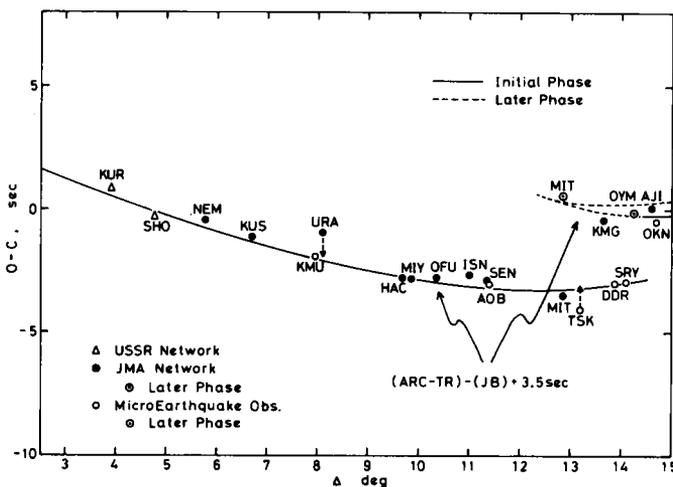

Figure 14. Observed travel-time residuals from JB times compared with the ARC—TR model for which a constant base line shift of 3.5 s is made.

uppermost mantle model affects our result only through the uncertainty of the depth estimation to stripe the earth. If there is some error in this estimation, each earth's radius associated with the velocity—depth profile will be in error by the same fraction but the features of the model suffer little change.

The high-velocity gradient near the base of the low-velocity zone terminates at a depth of 200 km, below which a very small negative veloctiy gradient follows. This near 'critical' situation immediately below 200 km explains the very weak C arrival. The depth interval 230—380 km is characterized by a gradual increase in velocity gradient which causes a focusing of energy at 22.5—23° as a large later arrival. However we have only two data to constrain this part of the mantle. In the layer thickness of 10—15 km near 390 km there is about 6 per cent increase in velocity. The near critical reflection from this sharp transition produces the strong D later arrival extending back to $\Delta = 13.5°$. At depths 440—520 km the velocity increases fairly rapidly, the total increase being about 4 per cent. The velocity gradient is not so high as to produce a large triplication of the E branch near 21.5° and could be even smaller than the model indicates. A much more rapid increase in velocity occurs in the depth interval 630—680 km. This major transition zone consists of about 7 per cent increase in velocity and is sharp, especially near its base. Such sharpness is related to the substantial extension of the retrograde branch F toward its reverse end ($\Delta = 19.5°$) The model also possesses a minor transition zone at depths around 740 km with a velocity increase of about 2 per cent. For the moment its presence is marginally suggested from the $dT/d\Delta$ behaviour near 26° and more careful amplitude study is required.
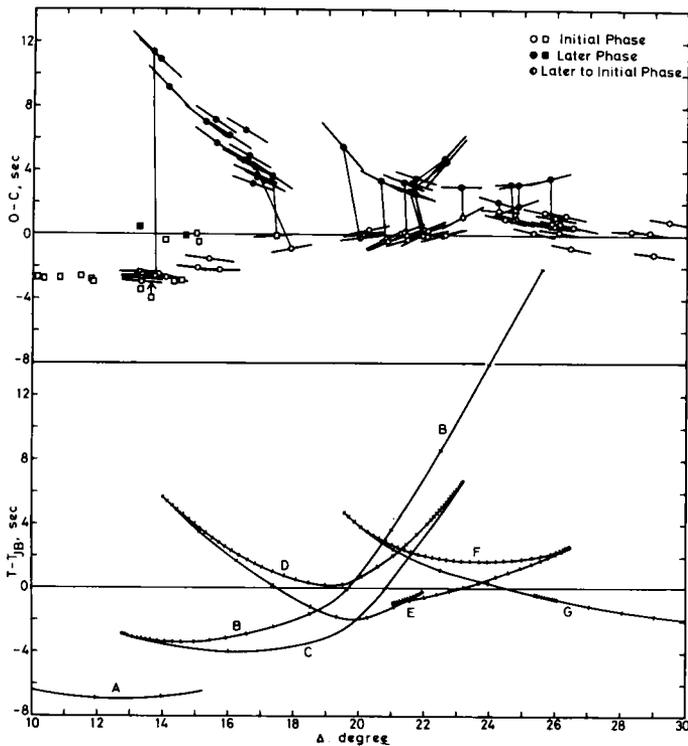

Figure 15. (Top) observed travel-time residuals and slownesses, corrected to surface focus. The first and later arrival data for a single event are connected with a line. The data for Event 64 are shown by squares. (Bottom), travel-time residuals calculated for the ARC—TR model. The travel curve is dotted with small bars according to the equal intervals of slowness (0.025s/deg).

The model presented in Fig. 13 and Table 3 is labelled ARC−TR. Since this model was constructed primarily on the basis of the $dT/d\Delta$ data, it is interesting to examine its consistency with the travel-time data. As discussed in the last section, however, the travel times based on the ISC locations may be sometimes in error by as much as 3−4 s. Moreover ARC−TR does not adequately describe the uppermost mantle just beneath the Wakayama net. We can therefore hardly expect a good agreement between the observed and theoretical travel times. It is more important to see to what extent the model is consistent with the observed relative times of the first and later arrivals.

Using the JB times as a reference, the travel-time data corrected to surface focus are plotted in Fig. 15 (top). Note that for later phases we have measured the relative arrival times rather than the onset times of the first motion which is in general less accurately recognized. Although in Fig. 15 the later arrival data are corrected to the onset time by referring to the original seismograms, they are in this sense less accurate than the first-arrival data. The first and the later arrival data derived from a single event are connected with a line to show their relative time separation. The thick bar attached to each travel-time point shows the measured value of slowness and the distance range involved in the measurement. For comparison we plotted in Fig. 15 (bottom) the travel times calculated for model ARC−TR. Although the observed and calculated travel times do not show a precise coincidence, presumably for the reason described above, the general trend is quite similar to each other. Both give, for the first arrival, the maximum residual $(T-T_{JB})$ near $\Delta=24°$. More remarkable is the agreement between the observed and the calculated relative times of the first and later arrivals. The agreement is also satisfactory for the crossover distances near $\Delta=20°$ and $\Delta=24-24.5°$. All of these are the verification of the ARC−TR model.

In Fig. 15 (bottom) the calculated travel-time curve is dotted with small bars according to the equal intervals of slowness (0.025 s/deg). The density of the bars gives a measure of $d^2T/d\Delta^2$ or the square of the geometrical spreading factor which is closely related to amplitudes. The amplification of the E branch at distances $21-22°$ is the result of the fairly rapid velocity increase near 500 km depth. The local amplification of the D branch at 22.5° occurs by the velocity−depth profile above the 400 km transition zone. The three major transition zones near 200, 400, and 650 km produce large amplitudes in the vicinity of their retrograde cusps. Such amplitude behaviours are evidenced by the observation.

6 Discussion

The model of the uppermost mantle was constructed primarily to determine the depth of striping the earth. The detail of this part of the mantle is obviously not resolvable from such very limited data as ours. For example, our lithospheric model gives an apparent velocity of 8.30 km/s over distances up to 14.5°. On the other hand the *Pn* velocity of 8.2 km/s is reported off Pacific coast of northern Japan and in the vicinity of the trench (e.g. Asada & Shimamura 1976). Near the coast the corresponding velocity is 8.0−8.1 km/s (Suzuki 1976). Asada & Shimamura (1976) obtained, in the vicinity of the trench, an apparent velocity of 8.6 km/s for the lower part of the lithosphere whose thickness was suggested to be relatively thin. These observations indicate a laterally and vertically heterogeneous lithosphere. We so hope that our model of the lithosphere will give a correct integrated feature of this complexity.

The low-velocity zone starts at a depth of 85 km. It possesses a relatively high average velocity of 8.10 km/s which is one of the important characteristics of the model. The overall feature of the low-velocity zone is similar to that proposed by Mizoue & Tsujiura (1974) from their $O-C$ studies. We note that the sample areas are slightly different at depths below and above 200 km although both areas are classified as a trench side. One is somewhat
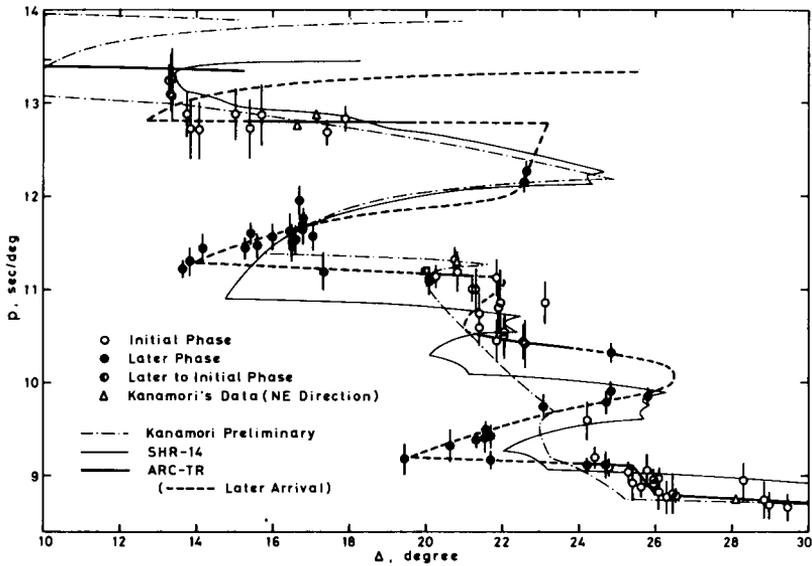
Figure 16. Comparison of the slowness data with three upper mantle models Preliminary (Kanamori 1967), SHR14 (Helmberger & Engen 1974) and ARC–TR.

further off coast than the other (see Figs 1 and 10). We have simply assumed that the velocities are the same at depths around 200 km for both areas. Fig. 13 compares ARC–TR to the Kanamori's (1967) Preliminary model. They are grossly different as far as the upper 200 km is concerned. ARC–TR is 1.4 s faster than Preliminary in terms of the two-way vertical travel time from surface down to 200 km. The difference can be attributed to the regionality. In this depth range Preliminary describes the uppermost mantle at the continental side of island arcs (Kanamori 1970) whereas ARC–TR at the trench side.

The velocity gradient is not positive but can be even almost critical just below the base of the low-velocity zone. A similar feature exists in model HWNE (Helmberger & Wiggins 1971) and model HWB (Wiggins & Helmberger 1973) which were constructed for the northern part of the western United States. The absence of a velocity increase at the corresponding depths was also suggested by Green & Hales (1968), White (1971) and Simpson, Mereu & King (1974) for the central United States, the Australian Shield and the northeastern Australia respectively. Underneath this particular zone the velocity gradient of ARC–TR gradually increases up to the depth of the 400 km transition which consists of about 6 per cent increase in velocity over a thickness of less than 15 km. This amount of velocity increase is consistent with the Kanamori model but is smaller than that for some of the recent upper mantle models such as SHR14 (Helmberger & Engen 1974, see Fig. 13). The velocity of SHR14 is too high at the bottom of the 400-km transition to be consistent with our slowness data (Fig. 16). The sharpness of this transition is also noted. Although the transition zone is not sharp enough to produce the short-period $P'_{400}P'$ phase (Whitcomb & Anderson 1970; Adams 1971), this simply means that the thickness of the transition is not less than 5 km (Richards 1972; Nakanishi & Fukao, in preparation). A thickness of about 10 km is therefore consistent with both the results of our study and the $P'dP'$ studies. The complicated amplitude behaviour of the later arrivals from the 400-km transition has been left unexplained.

The velocity of ARC–TR increases by about 4 per cent in the depth range 440–520 km. This feature is similar to that for models HWA and HWB (Wiggins & Helmberger 1973)

which have a velocity increase of about 3 per cent at depths 440—530 km. Our model shows a marked velocity increase near 650 km. Although the Kanamori model does not show such a feature, he suggested that the actual velocity variation can be sharper than that his model indicated. In fact Kurita & Inadani (1975) found a later phase branch related to the 650-km transition for the travel paths from Taiwan to the Wakayama Observatory. It is now therefore almost certain that the 650-km transition exists both at the trench side and the continental side of island arcs. The total increase in velocity is about 7 per cent and is mid-way between those of CIT204 (Johnson 1967) and SHR14 (Helmberger & Engen 1974, see Fig. 13). The 650-km transition of ARC—TR is sharp especially near the base of the zone. This bottom part can be still sharper and may be responsible for the clear arrivals of $P'_{650}P'$.

Figs 13 and 16 compare ARC—TR to Preliminary (Kanamori 1967) and SHR14 (Helmberger & Engen 1974). In the depth range 200—800 km an appropriately smoothed version of ARC—TR gives a feature similar to Preliminary. The two-way vertical travel time from 200 to 800 km is 126.0 s for ARC—TR and 126.2 s for Preliminary, the difference being just minor. On the other hand SHR14 gives the corresponding travel time 0.9 s shorter than ARC—TR since SHR14 is significantly faster than ARC—TR at depths 400—650 km. Such a high-velocity model is not consistent with our slowness data as shown in Fig. 16.

7 Structural anomaly in the Kii Peninsula

In the process of the least-squares fitting to the arrival times we recognized that, for a given arrival, the residual has a tendency to be positive at WK and OI and negative at KK and HD. To show this more clearly a station anomaly is defined as a station average of the residuals
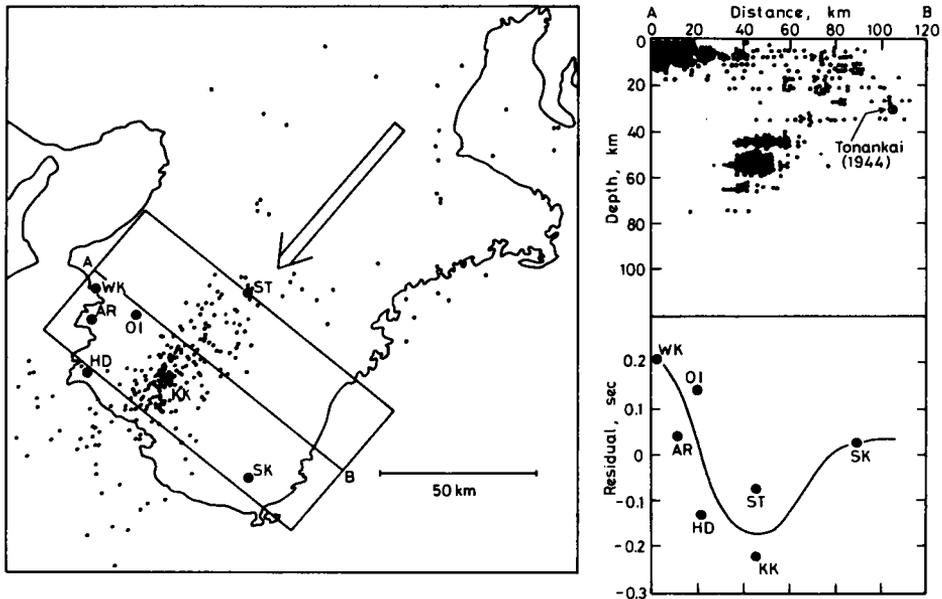

Figure 17. (Left) deep earthquakes ($40 \leq h \leq 70$ km) that occurred during the period from 1966 January to 1969 July (after Tsumura 1972). Arrow shows the incident direction of the *P* waves from the Kurile—Kamchatka region. (Right-top) hypocentres of two groups of earthquakes (for 1969 January—July) that occurred in the rectangular area shown in the left figure (after Kanamori 1972). The plane of projection is taken at AB. The hypocentre of the 1944 Tonankai earthquake is shown for reference. (right-bottom) Correlation of the station anomalies with the hypocentre distribution shown in the figure on the top.

for the least-squares determinations of $dT/d\Delta$. The anomaly in seconds calculated for the first arrivals is 0.01 ± 0.18(IS), 0.02 ± 0.20(IN), −0.09 ± 0.19(HB), 0.02 ± 0.23(KU), −0.07 ± 0.27(ST), 0.14 ± 0.29(OI), 0.21 ± 0.29(WK), −0.22 ± 0.20(KK), 0.04 ± 0.25(AR), 0.03 ± 0.21(SK) and −0.13 ± 0.20(HD). Although the standard deviation is at least as large as the mean value, the positive anomaly at WK and OI and the negative anomaly at KK and HD are clearly indicated. The station anomaly for the later arrivals shows the same tendency.

This phenomenon appears to be related to the seismicity in the Kii peninsula where local earthquakes can be classified into distinct groups (Kanamori & Tsumura 1971). One is a group of shallow ($h \le 10$ km) earthquakes on the western coast of the peninsula. The second is a group of mantle earthquakes ($30 \le h \le 70$ km) whose epicenters are shown in Fig. 17 (left) (Tsumura 1972). Kanamori (1972) projected the hypocenters of the above two groups of earthquakes occurring in such an area as shown in Fig. 17 (left) onto the vertical plane taken at AB (Fig. 17, right-top). The figure clearly shows the spatial difference between the two groups. Note that the ray paths for *P* waves from the Kurile−Kamchatka region are almost vertical in this projection. Among the seven stations in this area, WK is situated on the most dense cluster of the first group of earthquakes and OI is on its border. Station KK is situated right above the most intense cluster of the second group of earthquakes and HD is above its western extension. Fig. 17 (right-bottom) shows how the seismic activity near a station relates to the station anomaly. The positive station anomaly is closely related to the very shallow earthquake cluster and the negative station anomaly to the mantle earthquake cluster. Such correlation may have an important bearing on the nature of two groups of earthquakes. If the station anomalies obtained above were incorporated in the slowness determination, the standard deviation would be in general slightly reduced but the slowness value itself would be little affected.

8 Conclusions

A greater number of data have been accumulated at the Wakayama Micro-Earthquake Observatory since Kanamori's (1967) $dT/d\Delta$ study. This enabled us to sample the data from a tectonically well-defined region. The non-uniqueness was considerably reduced by including later arrival data. The resultant model ARC−TR describes the upper mantle structure on the oceanic or trench side of the Japan−Kurile arc. The model may also be used as a first approximation for the mantle beneath the farthest part of the Pacific Ocean from the mid oceanic ridge. The lithosphere is thicker and the low-velocity layer is faster than those of the recent average oceanic model (Anderson & Hart 1976). The velocity does not increase with depth just beneath the base of the low-velocity zone. Below 200 km depth there are two major transition zones near 400 and 650 km and two minor transition zones near 500 and 750 km. The 400-km transition is not so broad at least in Japan and Kurile as Simpson *et al.* (1974) proposed. The 650-km transition is not so small as that of SHR14 (Helmberger & Engen 1974). Mineralogical implications of these results will be discussed elsewhere incorporating the results of our recent study of $P'dP'$ phase (Nakanishi & Fukao, in preparation).

Kenshiro Tsumura, Tetsuo Takanami, and Shigeki Horiuchi who kindly sent me the copies of the seismograms. Useful discussions with Drs Tokuji Utsu and Harumi Aoki are acknowledged. The final version of this paper was written while I was a Geophysical Research Fellow at Seismological Laboratory, California Institute of Technology. I am grateful for Drs Don L. Anderson, Hiroo Kanamori, and Donald V. Helmberger, who kindly read the manuscript and gave me various comments.

References

Adams, R. D., 1971. Reflections from discontinuities beneath Antarctica, *Bull. seism. Soc. Am.,* **61,** 1441–1451.

Anderson, D. L. & Hart R. S., 1976. An earth model based on free oscillations and body waves, *J. geophys. Res.,* 81, 1461–1475.

Asada, T. & Shimamura, H., 1976. Observation of earthquakes and explosions at the bottom of the western Pacific: Structure of oceanic lithosphere revealed by longshot experiment, in *The geophysics of the Pacific Ocean basin and its margin,* eds G. P. Woolard, G. H. Sutton, M. H. Manghanani & R. Moberly, Am. geophys. Un. Monogr. No. 19.

Green, R. W. E. & Hales A. L., 1968. The travel times of *P* waves to 30° in the central United States and upper mantle structure, *Bull. seism. Soc. Am.,* 58, 267–289.

Hamada, K., 1973. The upper mantle beneath Japan inferred from *P* travel-time anomalies by means of three dimensional ray tracing: Part 1, *J. Phys. Earth,* 21, 463–474.

Helmberger, D. & Wiggins R. A., 1971. Upper mantle structure of midwestern United States, *J. geophys. Res.,* 76, 3229–3245.

Helmberger, D. V. & Engen G. R., 1974. Upper mantle shear structure, *J. geophys. Res.,* 79, 4017–4028.

Hirono, T., 1959. The Etorofu-Oki earthquake of November 7, 1958 (in Japanese), *Kenshinjiho (Quart. J. Seism.),* 24, 1–25.

Johnson, L. R., 1967. Array measurements of *P* velocities in the upper mantle, *J. geophys. Res.,* 72, 6309–6325.

Kanamori, H., 1967. Upper mantle structure from apparent velocities of *P* waves recorded at Wakayama Micro-Earthquake Observatory, *Bull. earthquake Res. Inst. Tokyo Univ.,* 45, 657–678.

Kanamori, H., 1970. Mantle beneath the Japanese arc, *Phys. Earth planet. Int.,* 3, 475–483.

Kanamori, H., 1972. Tectonic implications of the 1944 Tonankai and the 1946 Nankaido earthquakes, *Phys. Earth planet. Int.,* 5, 129–136.

Kanamori, H. & Tsumura K., 1971. Spatial distribution of earthquakes in the Kii peninsula, Japan, south of the Median Tectonic Line, *Tectonophys.,* 12, 327–342.

Kelleher, J., Sykes, L. & Oliver J., 1973. Possible criteria for predicting earthquake locations and their application to major plate boundaries of the Pacific and the Caribbean, *J. geophys. Res.,* 78, 2547–2585.

Kishimoto, Y., 1951. On a 13° – discontinuity of the earth's mantle (in Japanese), *Zisin 2nd Ser.,* 5, 7–12.

Kishimoto, Y., 1956. Seismometric investigation of the earth's interior, Part 3. On the structure of the earth's mantle (I), *Mem. Coll. Sci. Kyoto Univ. Ser. A,* 28, 117–142.

Kurita, K. & Inadani H. 1975. Upper mantle beneath Japan (in Japanese), *Abstract for Ann. Meet. seism. Soc. Japan.*

Mizoue, M. & Tsujiura M., 1974. Azimuthal Variation of Upper mantle structure from *P*-wave travel time residuals at Dodaira Micro-Earthquake Observatory (in Japanese), *Kenkyusokuho* (Earthquake Res. Inst. Tokyo Univ.), 12, 57–71.

Niazi, M., 1966. Corrections to apparent azimuths and travel-time gradients for a dipping Mohorovicic discontinuity, *Bull. seism. Soc. Am.,* 56, 491–509.

Richards, P. G., 1972. Seismic waves reflected from velocity gradient anomalies within the earth's upper mantle, *Z. Geophys.,* 38, 517–526.

Simpson, D. W., Mereu R. F. & King D. W., 1974. An array study of *P*-wave velocities in the upper mantle transition zone beneath northeastern Australia, *Bull. seism. Soc. Am.,* 64, 1757–1788.

Suzuki, S., 1976. Lateral variation of *P* wave velocity in the upper mantle beneath Northern Japan, as derived from travel times of earthquakes (in Japanese), *Zisin,* 29, 99–116.

Tsumura, K. (1972). Microearthquakes in Wakayama Prefecture (in Japanese), in *Report on seismic activity in Wakayama Prefecture,* Earthquake Res. Inst., Tokyo University.

Utsu, T., 1971. Anomalous structure of the upper mantle beneath the Japanese islands (in Japanese), *Geophys. Bull. Hokkaido Univ. Japan,* 25, 99–128.

Utsu, T., 1975. Regional variation of travel-time residuals of P waves from nearby deep earthquakes in Japan and vicinity, *J. Phys. Earth*, 23, 367–380.

Whitcomb, J. H. & Anderson D. L., 1970. Reflection of p' p' seismic waves from discontinuities in the mantle, *J geophys. Res.*, 75, 5713–5728.

White, R. E., 1971. *P*-wave velocities in the upper mantle beneath the Australian Shield from earthquake data, *Geophys. J. R. astr. Soc.*, 24, 109–118.

Wiggins, R. A. & Helmberger D. V., 1973. Upper mantle structure of the western United States, *J. geophys. Res.*, 78, 1870–1880.